# Metastability and Nucleation in Capillary Condensation

Frédéric Restagno, Lydéric Bocquet, and Thierry Biben

*Laboratoire de Physique (UMR CNRS 5672), ENS-Lyon, 46 allée d'Italie, 69364 Lyon Cedex 07, France*

(Received 19 January 1999)

This paper is devoted to thermally activated dynamics of capillary condensation. On the basis of a simple model we identify the critical nucleus involved in the transition mechanism and calculate the nucleation barrier from which we obtain information on the nucleation time. Close to the condensation point, the theory predicts extremely large energy barriers leading to strong metastabilities, long time dependencies, and large hysteresis in agreement with experimental observations in mesoporous media. The validity of the model is assessed using a numerical simulation of a time-dependent Ginzburg-Landau model for the confined system.

PACS numbers: 64.60.Qb, 64.70.Fx, 68.10.Jy

Porous materials are involved in many physical, chemical, or biological processes. Their porosities confer to these materials the property of being natural reservoirs for water, oil, or gas. Their adsorption properties are known to present a variety of behaviors related to the texture of the porous matrix, which provides an experimental way to analyze the pore size distribution. Interpretation of adsorption isotherms in these materials commonly invokes a well known phenomenon, capillary condensation [1,2], which corresponds to the condensation of liquid bridges in the pores. More fundamentally, capillary condensation is a gas-liquid phase transition shifted by confinement. A basic model of confinement is provided by the slab geometry, for which the fluid is confined between two parallel planar solid walls. The classical macroscopic theory based on this model [2] predicts a condensation of the liquid phase, when the substrate-liquid surface tension $\gamma_{SL}$ is smaller than the substrate-vapor surface tension $\gamma_{SV}$, below a critical distance $H_c$ between the solid surfaces satisfying the Kelvin equation, $\Delta\rho\Delta\mu \simeq 2(\gamma_{SV} - \gamma_{SL})/H_c$. Here, $\Delta\rho = \rho_L - \rho_V$ is the difference between the bulk densities of the liquid and the gas phase, $\Delta\mu = \mu_{\rm sat} - \mu$ is the (positive) undersaturation in chemical potential, and $\mu_{\rm sat}$ is the chemical potential at bulk coexistence. Although the equilibrium properties of this transition have motivated many experimental [3,4] and theoretical studies [2,5,6], capillary condensation presents remarkable dynamical features which are still to be explained. The most striking feature is the huge metastability of the coexisting phases, which contrasts with the bulk liquid-vapor transition. This behavior manifests itself, for example, in the existence of hysteresis loops in adsorption isotherms of gases in mesoporous solids [5], or in well controlled measurements using surface force apparatus techniques [4]. A related observation concerns the extremely long time scales measured in the adsorption process, as measured, e.g., in cement pastes and concretes [7], or in the humidity dependent aging behavior of granular media [8]. A detailed description of the dynamics providing an estimate of the condensation time is thus still needed.

Since capillary condensation is a first order phase transition, one should be able to identify a critical nucleus and a corresponding free-energy barrier (away from the spinodal line [9]). In this Letter we show that, as in the homogeneous nucleation case, the shape of the critical nucleus results from the balance between surface and volume contributions. To test this picture, we shall consider a simplified model keeping only the main ingredients for capillary condensation, and compare our results to numerical simulations of the activated dynamics.

In the grand-canonical ensemble the critical nucleus corresponds to a saddle point of the grand potential. We will consider in this Letter the perfect wetting situation $\gamma_{SV} = \gamma_{SL} + \gamma_{LV}$, although a generalization to the partial wetting case is straightforward. The grand potential of a pore partially filled with liquid may be written [2] $\Omega = -p_V V_V - p_L V_L + \gamma_{SV} A_{SV} + \gamma_{SL} A_{SL} + \gamma_{LV} A_{LV}$, where $V_V$ ($V_L$) is the volume of the gas (liquid) phase and $A_{SL}$, $A_{SV}$, and $A_{LV}$, respectively, denote the total solid-liquid, solid-vapor, and liquid-vapor surface area. Our prescription for the grand potential is macroscopic in nature; i.e., we shall neglect the $H$ dependencies of the surface tensions. Using $\gamma_{SV} - \gamma_{SL} = \gamma_{LV}$ in the perfect wetting case, the following expression is obtained for the "excess" grand potential, $\Delta\Omega_{\rm tot} = \Omega - \Omega_V$, with $\Omega_V$ the grand potential of the system filled with the gas phase only:

$$\Delta\Omega_{\rm tot} = \gamma_{LV} A_{LV} + \gamma_{LV} A_{SL} + \Delta\mu\Delta\rho V_L , \qquad (1)$$

where we have used $p_V - p_L \simeq \Delta\rho\Delta\mu$. One expects the critical nucleus to exhibit rotational invariance, so that $\Delta\Omega_{\rm tot}$ in Eq. (1) is best parametrized in cylindrical coordinates (see Fig. 1b). In terms of $\rho(z)$, the position of the $L$-$V$ interface, one obtains

$$\begin{aligned}\Delta\Omega_{\rm tot} = {} & \Delta\rho\Delta\mu 2\pi \int_0^{H/2} dz\, \rho^2(z) \\ & + 2\gamma_{LV}\pi\rho^2\left(\frac{H}{2}\right) \\ & + 2\pi\gamma_{LV}\int_0^{H/2} dz\, \rho(z)\sqrt{1 + \rho_z^2}, \qquad (2)\end{aligned}$$

  

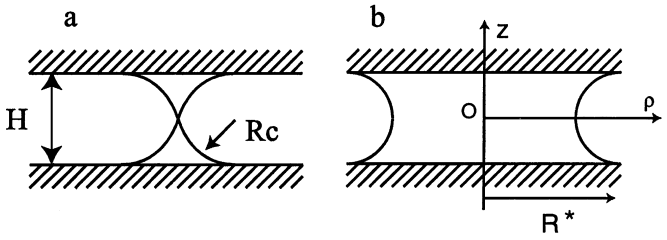


FIG. 1. The critical nucleus for capillary condensation in two dimensions (a), and three dimensions (b). $R^*$ represents the lateral extension of the critical nucleus (see text for details). The total curvature $\kappa$ of the meniscus is equal to $\kappa = 1/R_c = 2/H_c$. Note that, in 3D, $\kappa$ is the sum of the in-plane and "axisymmetric" (out-of-plane) curvature.

where the index $z$ denotes differentiation. Extremalization of the grand potential (2) leads to the usual condition of *mechanical equilibrium*, the Laplace equation, which relates the local curvature $\kappa$ to the pressure drop according to $\gamma_{LV}\kappa = \Delta p \simeq \Delta\mu\Delta\rho$. This condition remains valid although the nucleus corresponds to a saddle point of the grand potential.

The main difference with homogeneous nucleation comes from the pressure drop at the interface: here, the liquid pressure inside the meniscus is lower than the gas pressure since $\mu < \mu_{\rm sat}$, so that one expects the critical nucleus to take the form of a liquid bridge between the solid substrates instead of a sphere as in homogeneous nucleation (see Fig. 1b). The previous Laplace equation is nonlinear and cannot be solved analytically. From dimensional arguments, however, one expects $\Delta\Omega_{\rm tot} = \gamma_{LV}H_c^2 f(H/H_c)$, with $f(x)$ a dimensionless function. The latter can be obtained from the numerical resolution of the Laplace equation, yielding the shape of the meniscus [10]. Numerical integration of Eq. (2) then gives the corresponding free-energy barrier. The result for the energy barrier $\Delta\Omega^\dagger$ is plotted in Fig. 2. As can be seen from the figure, a divergence of $\Delta\Omega^\dagger$ is obtained as the pore width $H$ reaches $H_c$. When the extension of the bridge $R^* = \rho(\frac{H}{2})$ is large compared to $H$, the negative (axisymmetric) contribution to the curvature is negligible and the *L-V* profile can be approximated by a semicircular shape. This allows one to obtain explicit expressions for the different contributions to $\Delta\Omega_{\rm tot}$ in Eq. (1) as a function of the extension of the bridge $R^*$, namely, $V_L = \pi R^{*2}H - \frac{\pi^2}{4}R^*H^2 + \frac{\pi}{6}H^3$, $A_{SL} = 2\pi R^{*2}$, and $A_{LV} = \pi^2 R^* H - \pi H^2$. Maximization of $\Delta\Omega_{\rm tot}$ as a function of $R^*$ yields the following expression for the free energy barrier:

$$\Delta\Omega^\dagger = \gamma_{LV}H^2\left[\frac{\pi^3}{8}\frac{(1-\frac{H}{2H_c})^2}{1-\frac{H}{H_c}} - \left(-\frac{\pi}{3}\frac{H}{H_c} + \pi\right)\right], \tag{3}$$

which does exhibit a divergence at $H \sim H_c = 2\gamma_{LV}/\Delta\rho\Delta\mu$.

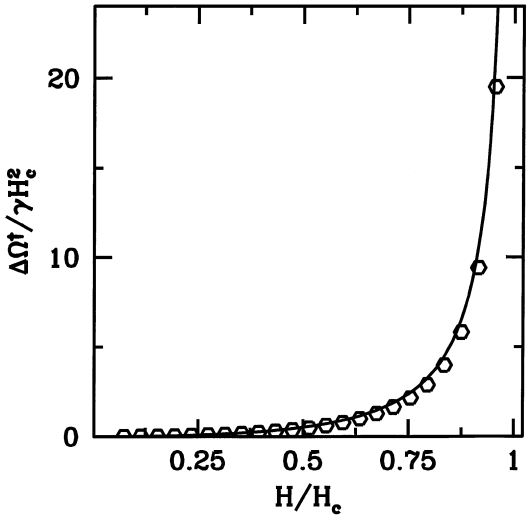


FIG. 2. Free energy barrier (in 3D) as a function of the normalized width of the pore, $H/H_c$. The solid line is computed by numerical integration of the Laplace equation. The points are obtained from the analytical expression, Eq. (3).

As shown in Fig. 2, this result is in very good agreement with the numerical estimate, even at small confinement $H$. Physically, an important consequence of the diverging energy barrier at $H_c$ is that the gas phase becomes extremely metastable. Thus, for the problem of adsorption of gases in mesoporous media, one expects extremely long adsorption time when the gas pressure $P_V$ (which fixes $\Delta\mu$) is such that $H_c(P_V)$ is of the order of the typical pore size $\bar{H}$, which is indeed observed experimentally [4,7]. Furthermore, this point is corroborated by the existence of large hysteresis loops in the adsorption of gases in mesoporous media [5].

If we now consider the more realistic situation where a long range van der Waals interaction exists between the substrates and the fluid, both distances $H$ and $H_c$ appearing in Eq. (3) [and Eq. (4) below] have to be modified to account for the finite thickness $\ell$ of the wetting films now condensed on the two surfaces, and for the modification of the nucleus profile. It can be shown that a $1/z^3$ potential can be accounted for provided the bare distance $H$ is replaced by $H - 3\ell$ (same for $H_c$) in the analysis presented above [5,11].

The previous model uses macroscopic concepts (such as surface tensions) to derive an energy barrier. In the case of homogeneous nucleation, it has been shown in numerical simulations that this gives essentially the correct qualitative behavior [12]. This can be verified using numerical simulations of the activated dynamics. As the latter involve a huge amount of computer time, data could be obtained only in 2D. We will therefore restrict the comparison to this case. We emphasize that this is, however, sufficient to assess the general validity of macroscopic considerations.

Before turning to the simulations, we quote the theoretical predictions for the 2D case. The theoretical approach

follows essentially the same lines as in the 3D case. The main difference lies in the absence of the azimuthal curvature in the 2D case and the mechanical equilibrium condition thus imposes a circular shape of the liquid-vapor interface, with a fixed radius of curvature $R_c = H_c/2$. As a consequence, the critical meniscus takes the form depicted in Fig. 1a corresponding to a liquid bridge with a vanishingly small lateral extension in $e = H/2$. The cusp in the center originates in the assumption of an infinitesimally thin *L*-*V* interface in the macroscopic picture. The corresponding energy barrier (per unit length in the perpendicular direction) is then obtained to be

$$\Delta\Omega^{\dagger} = \frac{4}{3}(\Delta\mu\Delta\rho\gamma_{LV})^{1/2}H^{3/2}. \tag{4}$$

As discussed above, the distance $H$ should be replaced by $H - 3\ell$ in the presence of a $1/z^3$ confining potential.

Simulations are based on a mesoscopic Landau-Ginzburg model for the grand potential of the 2D system confined between two walls. In terms of the local density $\rho(r)$, we write the excess part of the grand potential $\Omega^{\mathrm{ex}} = \Omega + P_{\mathrm{sat}}V$, where $P_{\mathrm{sat}}$ is the pressure of the system at coexistence, as

$$\Omega^{\mathrm{ex}} = \int dr\left\{\frac{m}{2}|\nabla\rho|^2 + W(\rho) + [\Delta\mu + V_{\mathrm{ext}}(z)]\rho\right\}. \tag{5}$$

In this equation, $m$ is a phenomenological parameter; $V_{\mathrm{ext}}(z)$ is the confining external potential, which we took for each wall as $V_{\mathrm{ext}}(z) = -\epsilon[\sigma/(\Delta z + \sigma)]^3$, with $\Delta z$ the distance to the corresponding wall; $\epsilon$ and $\sigma$ have the dimensions of an energy and a distance. It must be noted that this potential is not the actual van der Waals potential in 2D, but this choice will allow us to test the $H - 3\ell$ prescription. $W(\rho)$ can be interpreted as the negative of the excess pressure $\mu_{\mathrm{sat}}\rho - f(\rho) - P_{\mathrm{sat}}$, with $f(\rho)$ the bulk free-energy density [13]. As usual, we assume a phenomenological double well form for $W(\rho)$: $W(\rho) = a(\rho - \rho_V)^2(\rho - \rho_L)^2$, where $a$ is a phenomenological parameter [14]. The system is then driven by a nonconserved Langevin equation for $\rho$,

$$\frac{\partial\rho}{\partial t} = -\Gamma\frac{\delta\Omega^{\mathrm{ex}}}{\delta\rho} + \eta(r,t), \tag{6}$$

where $\Gamma$ is a phenomenological friction coefficient and $\eta$ is a Gaussian noise field related to $\Gamma$ through the fluctuation-dissipation relationship [15]. An equivalent model has been successfully used for the (bulk) classic nucleation problem [16]. We solved (6) by numerical integration using standard methods, identical to those of Ref. [16]. The units of energy and length are such that $\sigma = \epsilon = 1$. Time is in units of $t_0 = (\Gamma\epsilon\sigma^2)^{-1}$ with $\Gamma = \frac{1}{3}$. In these units, we took $m = 1.66$, $a = 3.33$, $\rho_L = 1$, and $\rho_V = 0.1$. Typical values of the chemical potential and temperature are $\Delta\mu \sim 0.016$, $T \sim 0.06$ (which is roughly half the critical temperature in this model). Periodic boundary conditions with periodicity $L_x$ were applied in the lateral direction. Typically $L_x \sim 2H$ was used, but we have checked that increasing $L_x$ up to $20H$ does not affect the results for the activation dynamics. We emphasize that this lack of sensitivity is not obvious since it is known that the amplitude of capillary waves increases with the lateral dimension of the system for *free interfaces* [2]. In our case, however, the long-range effects of the fluctuations of the liquid film are expected to be screened due to the presence of the external potential. Moreover, as predicted by the model, nucleation should occur via the excitation of localized fluctuations. The observed insensitivity of the results with respect to finite size effects is then an encouraging feature for the model presented above.

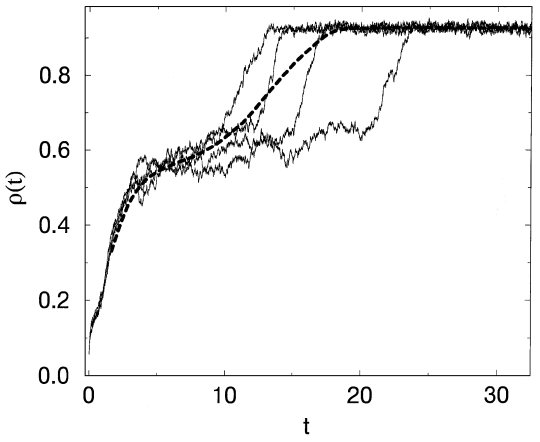


FIG. 3. Averaged density as a function of time $t$ (in units of $t_0$) for a few realizations of the noise ($H = 13$, $\Delta\mu = 0.016$, and $T = 0.07$). The dashed line is the average over all the realizations, $\bar{\rho}(t)$.

The simulated system is initially a gas state filling the whole pore, and its evolution is described by Eq. (6). A

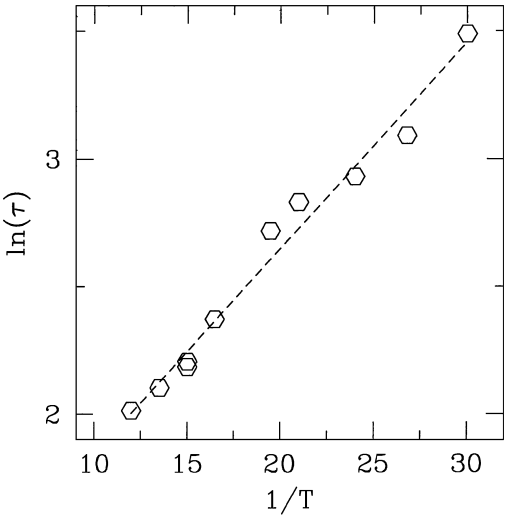


FIG. 4. Logarithm of condensation time as a function of the inverse temperature ($\Delta\mu = 0.016$, $H = 13$). The dashed line is a least-squares fit of the data.

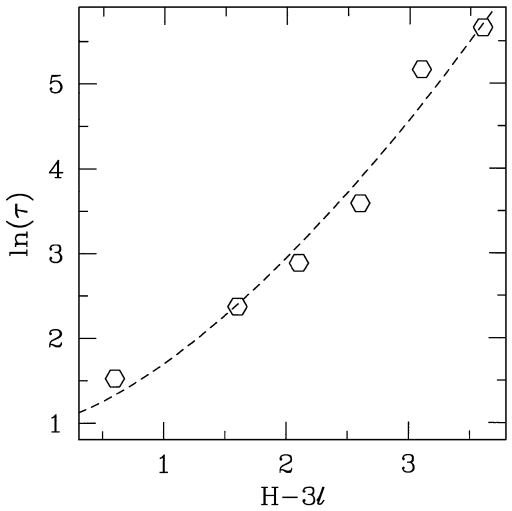


FIG. 5. Logarithm of condensation time as a function of the "effective" width of the slab $H - 3\ell$ for fixed $\Delta\mu = 0.016$. The dashed line is the theoretical prediction $\ln(\tau) = \ln(\tau_0) + \alpha(H - 3\ell)^{3/2}$. The two parameters $\ln(\tau_0)$ and $\alpha$ have been obtained from a least-squares fit of the data in a $\ln(\tau)$ versus $(H - 3\ell)^{3/2}$ plot.

typical evolution of the mean density in the slit $\rho(t)$ is plotted in Fig. 3. An average over different realizations (from 10 to 30) is next performed to get an averaged time-dependent density $\bar{\rho}(t)$. As expected [5], due to the long-range nature of the external potential a thick liquid film of thickness $\ell$ rapidly forms on both walls on a short time scale $\tau_1$ ($\ell \simeq 3.8\sigma$ and $\tau_1 \approx 5t_0$ in our case). In a second stage, fluctuations of the interfaces around their mean value $\ell$ induce after a while a sudden coalescence of the films (see Fig. 3). This second process has a characteristic time $\tau$. It is numerically convenient to define the total coalescence time, $\tau_1 + \tau$, as the time for the average density in the slab between the two wetting films to reach $(\rho_V + \rho_L)/2$ [16], which corresponds in our case to the condition $\bar{\rho}(\tau + \tau_1) \approx 0.8$. The physical results do not depend anyway on the precise definition of $\tau$.

In Fig. 4, we plot the variation of $\ln(\tau)$ as a function of the inverse temperature $1/T$. As expected, far from the spinodal (i.e., for large enough $H$, $H \gtrsim 3\ell$), $\tau$ is found to obey an Arrhenius law $\tau = \tau_0 \exp(\Delta\Omega^\dagger/k_B T)$, where $\Delta\Omega^\dagger$ is identified as the energy barrier for nucleation.

The $H$ dependence ($\Delta\mu$ being fixed) is plotted in Fig. 5. From Eq. (4), one expects $\ln(\tau) = \ln(\tau_0) + \alpha(H - 3\ell)^{3/2}$, with $\alpha = 4/3(\Delta\mu\Delta\rho\gamma_{LV})^{1/2}/kT$. As seen in Fig. 5, a good agreement with this theoretical prediction is found. The prefactor $\alpha$ can be independently estimated from the data plotted in Figs. 4 or 5, yielding $\alpha = 0.67$ (Fig. 4) and $\alpha = 0.68$ (Fig. 5), while the theoretical prediction gives $\alpha = 1.03$ (where the liquid-vapor surface tension—at finite temperature $T = 0.06$—has been computed from independent Monte Carlo simulations of the model, yielding $\gamma_{LV} = 0.8$). The macroscopic theory thus gives a correct qualitative picture and only a semiquantitative agreement. This slight overestimation of the macroscopic nucleation theory has also been observed in the homogeneous nucleation case [12].

The simulations thus show that, although the system is strongly confined, the macroscopic picture is valid to describe the critical nucleus for capillary condensation. Beyond the obtained results, many questions remain to be discussed, one of crucial importance being the role of roughness in the condensation process, in order to discuss adsorption kinetics in porous or granular media.

The authors thank E. Charlaix, J. Crassous, and J. C. Geminard for many interesting discussions. This work has been partly supported by the PSMN at ENS-Lyon, and the MENRT under Contract No. 98B0316.

[1] J. N. Israelachvili, *Intermolecular and Surface Forces* (Academic Press, London, 1985).
[2] R. Evans, in *Liquids and Interfaces,* edited by J. Charvolin, J. F. Joanny, and J. Zinn-Justin (Elsevier Science Publishers B.V., New York, 1989).
[3] L. R. Fisher and J. N. Israelachvili, J. Colloid Interface Sci. **80**, 528 (1980); H. K. Christenson, J. Colloid Interface Sci. **121**, 170 (1988).
[4] J. Crassous, E. Charlaix, and J. L. Loubet, Europhys. Lett. **28**, 37 (1994).
[5] R. Evans, U. Marini Bettolo Marconi, and P. Tarazona, J. Chem. Phys. **84**, 2376 (1986); R. Evans and U. Marini Bettolo Marconi, Chem. Phys. Lett. **114**, 415 (1985).
[6] B. V. Derjaguin, Prog. Surf. Sci. **40**, 46 (1992).
[7] V. Baroghel-Bouny, *Caractérisation des pâtes de ciment et des bétons* (Laboratoire Central des Ponts et Chaussées, Paris, 1994).
[8] L. Bocquet, E. Charlaix, S. Ciliberto, and J. Crassous, Nature (London) **396**, 735 (1998).
[9] For sufficiently small $H$, it can be shown that the liquid films coating the solid surfaces become unstable due to fluid-fluid interactions and grow to fill the slab (see Ref. [4] for details).
[10] W. H. Press, S. A. Teukolsky, W. T. Vetterling, and B. P. Flannery, *Numerical Recipes* (Cambridge University Press, Cambridge, 1992).
[11] J. Crassous, Thèse de Doctorat, E.N.S. Lyon, 1995.
[12] P. R. ten Wolde and D. Frenkel, J. Chem. Phys. **109**, 9901 (1998).
[13] J. S. Rowlinson and B. Widom, *Molecular Theory of Capillarity* (Oxford University Press, Oxford, 1989).
[14] S. A. Safran, *Statistical Thermodynamics of Surfaces, Interfaces, and Membranes* (Addison-Wesley Publishing Company, New York, 1994).
[15] P. M. Chaikin and T. C. Lubensky, *Principles of Condensed Matter Physics* (Cambridge University Press, Cambridge, 1995).
[16] O. T. Valls and G. F. Mazenko, Phys. Rev. B **42**, 6614 (1990).